

Length mismatch in random semiconductor alloys. II. Structural characterization of pseudobinaries

Y. Cai and M. F. Thorpe

*Department of Physics and Astronomy, Michigan State University, East Lansing, Michigan 48824
and Center for Fundamental Materials Research, Michigan State University, East Lansing, Michigan 48824*

(Received 26 May 1992)

We have made an extensive study of the pseudobinary semiconductor compounds $(A_{1-x}B_x)C$, which includes both the III-V and the II-VI alloys. We use a Kirkwood model with all parameters derived from the elastic constants of the pure materials. It is shown that the mean lengths are *linear* in the composition x if the force constants for the two pure materials AC and BC are the same. We have derived analytic results for the mean lengths of AC and BC bonds and for their widths in the preceding paper. We construct an effective-medium theory for cases in which there is disorder in the force constants. This effective-medium theory is found to be in good agreement with the results of computer simulations of the same models. Mean values for the next-nearest-neighbor lengths are also given, and found to agree with extended x-ray-absorption fine-structure results.

I. INTRODUCTION

Structural information on semiconducting materials is of fundamental importance in calculating, predicting, and understanding their properties.¹⁻⁵ Extended x-ray absorption fine structure (EXAFS) experiments have found that pseudobinary semiconductor alloy systems $(A_{1-x}B_x)C$ exhibit a bimodal structure.²⁻⁶ The first-neighbor cation-anion distance remains closer to that in the pure binary compound than to that of the average or virtual crystal. This discovery inspired considerable theoretical interest.⁷⁻¹⁰ In this paper we apply the general results for quaternaries found in the preceding paper,¹¹ henceforth referred to as paper I, to the case of pseudobinary semiconducting alloys. Our statistical approach was shown to be successful in I by comparison with computer simulations. The model is also applicable to binary alloy systems like $\text{Si}_{1-x}\text{Ge}_x$ which will be studied in the following paper, paper III.¹² Our investigation provides a better understanding of the theoretical assumptions behind Vegard's law.¹ The layout of this paper is as follows. We first discuss the valence force models in Sec. II. The force constants of the models are fit from elastic measurements for known pure binary crystals, and we give extensive tables of these force constants. In Sec. III we apply the analytic results from paper I to ideal pseudobinary alloys (no force constant disorder). This result demonstrates the importance of the *topological rigidity constants*, which characterize the rigidity of the underlying lattice system. We also discuss the importance of the topological rigidity parameters in the construction of an effective-medium theory for use when there is *variation in the force constants*. In Sec. IV we study in considerable detail all pseudobinary III-V and II-VI semiconductor alloys using both effective-medium theory and computer simulations. Results are presented in a form that can be used for comparison with experimental data. We fo-

cus particularly on the deviations from straight lines for the mean lengths, caused by the force constant disorder. This bowing is much smaller than might have been expected. In general we find satisfactory agreement with experiment, where results are available.

II. VALENCE FORCE MODELS

Valence force models have been used to give a reasonable overall description of the phonons in semiconductors. In the diamond and zinc-blende structures, nearest-neighbor central force interactions alone lead to unstable structures that can be sheared. In fact one-third of the vibrational modes, which correspond to the transverse acoustic modes, have zero frequency. At a minimum some short-range angular interactions are needed to stabilize the structure. The Kirkwood¹³ and Keating¹⁴ potentials contain second-neighbor interactions which are sufficient to stabilize the zinc-blende structure. These models are adequate for our purpose and little would be gained by going to a more detailed force constant model. There are some subtle differences between the Kirkwood and the Keating models, although both can be regarded as providing simple two-parameter fits to the phonon dispersion relations in the pure binary materials. We have a preference for the Kirkwood model as it separates the angular forces from the bond-stretching forces in a clean way. This makes it easier to construct an effective-medium theory which is necessary if there is disorder in the force constants together with the length mismatch. We will only give the results from the Kirkwood model in the main part of this paper. A comparison of results from the Kirkwood and Keating models is given in the Appendix and Table I, where it is shown there that the differences between these two models are quite small.

We use the Kirkwood model¹³ as in I,

$$V = \frac{\alpha}{2} \sum_{\langle ij \rangle} (L_{ij} - L_{ij}^0)^2 + \frac{\beta}{8} L_e^2 \sum_{\langle ijil \rangle} (\cos \theta_{ijil} + \frac{1}{3})^2, \quad (1)$$

where the force constants α and β are the nearest neighbor and the angular force constant, respectively, L_{ij} is the bond length between atoms i and j , L_{ij}^0 is the natural (unstrained) bond length and θ_{ijil} is the angle between nearest-neighbor bonds ij and il . The angular brackets $\langle \dots \rangle$ under the summations exclude double counting.

The potential (1) can be expanded for small length mismatch. Denoting by L_e the nearest-neighbor distance of the underlying (undistorted) crystal structure, and \mathbf{u}_i the displacement vector of atom i from its crystalline position, and expanding up to linear terms,

$$L_{ij} = L_e + \hat{\mathbf{r}}_{ij} \cdot \mathbf{u}_{ij}, \quad (2)$$

where $\hat{\mathbf{r}}_{ij}$ is a unit nearest-neighbor vector in the perfect crystal structure pointing from atom i to j . The potential (1) can now be rewritten as

$$V = \frac{\alpha}{2} \sum_{\langle ij \rangle} (L_e - L_{ij}^0 + \hat{\mathbf{r}}_{ij} \cdot \mathbf{u}_{ij})^2 + \frac{\beta}{8} \sum_{\langle ijil \rangle} [\hat{\mathbf{r}}_{ij} \cdot \mathbf{u}_{il} + \hat{\mathbf{r}}_{il} \cdot \mathbf{u}_{ij} + \frac{1}{3}(\hat{\mathbf{r}}_{ij} \cdot \mathbf{u}_{ij} + \hat{\mathbf{r}}_{il} \cdot \mathbf{u}_{il})]^2. \quad (3)$$

In the perfect system, there is no length mismatch and $L_e = L_{ij}^0$, so that

$$V = \frac{\alpha}{2} \sum_{\langle ij \rangle} (\hat{\mathbf{r}}_{ij} \cdot \mathbf{u}_{ij})^2 + \frac{\beta}{8} \sum_{\langle ijil \rangle} [\hat{\mathbf{r}}_{ij} \cdot \mathbf{u}_{il} + \hat{\mathbf{r}}_{il} \cdot \mathbf{u}_{ij} + \frac{1}{3}(\hat{\mathbf{r}}_{ij} \cdot \mathbf{u}_{ij} + \hat{\mathbf{r}}_{il} \cdot \mathbf{u}_{il})]^2. \quad (4)$$

Using the method of Keating,¹⁴ the elastic constants of the Kirkwood model are found to be

$$\begin{aligned} C_{11} &= \frac{1}{4a} [\alpha + \frac{8}{3}\beta], \\ C_{12} &= \frac{1}{4a} [\alpha - \frac{4}{3}\beta], \\ C_{44} &= \frac{1}{4a} \left[\frac{36\alpha\beta}{9\alpha + 16\beta} \right], \end{aligned} \quad (5)$$

where $a = L_e/\sqrt{3}$. The frequency of the optic phonon at $\mathbf{k} = 0$ is

$$\omega_0 = \sqrt{\frac{4}{\mu} [\alpha + \frac{16}{9}\beta]}, \quad (6)$$

where μ is the reduced mass.

The force constants in the models are chosen to fit the elastic modulus C_{11} and the bulk modulus $B = \frac{1}{3}(C_{11} + 2C_{12})$.¹⁵ In Table I, we list the force constants for different zinc-blende compounds. In the Appendix and Table I we see that the angular force constants β are identical for both the Keating and Kirkwood models, while the central force constants α are different. We emphasize that the main reason that we adopt the Kirkwood

TABLE I. The force constants α and β (in N/m) for the Keating and Kirkwood models obtained from the elastic moduli, as described in the text.

	Kirkwood model		Keating model	
	α	β	α	β
AlP	65.03	14.19	60.30	14.19
AlAs	44.18	8.94	41.20	8.94
AlSb	35.69	6.79	33.42	6.79
GaP	48.06	10.69	44.50	10.69
GaAs	44.34	9.25	41.25	9.25
GaSb	34.29	7.33	31.85	7.33
InP	41.72	6.60	39.52	6.60
InAs	35.09	5.75	33.17	5.75
InSb	31.30	5.07	29.61	5.07
ZnS	40.30	4.78	38.70	4.78
ZnSe	33.74	4.56	32.22	4.56
ZnTe	31.06	4.66	29.51	4.66
CdS	35.66	4.75	34.07	4.75
CdSe	33.18	4.37	31.72	4.37
CdTe	27.30	2.72	26.39	2.72
HgTe	30.72	2.93	29.75	2.93

model is its simplicity when there is size mismatch in the system. As can be seen in Eq. (1), the length mismatch comes only in the central force part of the potential and *not* in the angular part.

The fitted force constants α and β shown in Table I give the shear modulus C_{44} and the optic mode frequency ω_0 with errors smaller than 20% for most compounds but up to around 40% for some other compounds when compared with experiments.¹⁵ Of course, it is possible to choose different angular force constants for *ABA* and *BAB* angles and this and other embellishments would lead to better fits to the elastic constants and the optic mode frequency. One could further consider the charge transfer and deploy a shell model. However, it is not necessary to fit every detail of the phonon dispersion curves, as *all* the phonons are involved in the concentration waves that lead to the structural distortions in the alloys. We find that even large variations in the force constants in the binaries at the two extreme compositions only lead to a very *small* bowing in the mean lengths, which is unobservable in most cases. Even in the most extreme case $\text{Zn}_{1-x}\text{Cd}_x\text{Te}$, the bowing is only just observable experimentally, as discussed in Sec. IV. This is why simple models like the Kirkwood and Keating models are adequate. Other approaches, such as using an embedded-atom po-

tential in metals, can only be studied using numerical simulation.¹⁶

III. THEORY

A. Analytic results

The general results for the quaternary alloys $A_{1-x}B_xC_{1-y}D_y$ found in paper I are applicable to the pseudobinary system $(A_{1-x}B_x)C$ by either equating the two chemical species $C = D$ and/or setting the concentration $y = 0$. From results presented in paper I, we have expressions for the average distance and length fluctuations for nearest neighbors, which now become

$$\langle L_\epsilon \rangle = L_e - \frac{a^{**}}{2}(\epsilon - 1 + 2x)(L_{BC}^0 - L_{AC}^0), \quad (7)$$

$$\langle L_\epsilon^2 \rangle - \langle L_\epsilon \rangle^2 = (a_1^{**} - a^{**2})x(1-x)(L_{BC}^0 - L_{AC}^0)^2, \quad (8)$$

where $L_e = (1-x)L_{AC}^0 + xL_{BC}^0 = r_A^0 + r_C^0 + x(r_B^0 - r_C^0)$. The additivity assumption (i.e., $L_{AC}^0 = r_A^0 + r_C^0$) is *unnecessary* for the pseudobinary alloys as there are only two natural lengths and a greater number (three) of atomic radii. In the quaternary alloys there are four natural bond lengths and an equal number (four) of atomic radii. We use the convention that $\epsilon = +1$ for A- and $\epsilon = -1$ for B-type atoms.

There are two different types of expressions for second-nearest-neighbor distances, one with a C atom in the center, and the other with a C atom at both ends. From the general theory of paper I, these are

$$\langle L \rangle_{\epsilon_1 \epsilon_2}^{iCj} = L_e^{\text{nnn}} - \sqrt{\frac{3}{8}}b^{**} \left(\frac{\epsilon_1 + \epsilon_2}{2} + 2x + 1 \right) \times (L_{BC}^0 - L_{AC}^0), \quad (9)$$

$$\langle L \rangle_\epsilon^{CiC} = L_e^{\text{nnn}} - \frac{1}{2}\sqrt{\frac{8}{3}}a^{**}(\epsilon + 2x - 1)(L_{BC}^0 - L_{AC}^0),$$

where the i, j are on A, B sublattices. The first of these equations involves only the topological rigidity constant b^{**} , while the second only involves a^{**} . The mean next-nearest-neighbor distance (averaged over all chemical species on both sublattices) is $L_e^{\text{nnn}} = \sqrt{8/3}L_e$. The average *angular* distortion associated with different configurations can be derived directly from the expressions (7)–(9).

If we write the nearest-neighbor mean distances and fluctuations in terms of dimensionless variables d ,^{17,18} defined by

$$d = \frac{L - L_{AC}}{L_{BC} - L_{AC}} \quad (10)$$

then the results (7) and (8) become

$$\begin{aligned} \langle d \rangle &= x, \\ \langle d_{AC} \rangle &= x(1 - a^{**}), \end{aligned} \quad (11)$$

$$\begin{aligned} \langle d_{BC} \rangle &= 1 - (1-x)(1 - a^{**}), \\ \langle d_{AC}^2 \rangle - \langle d_{AC} \rangle^2 &= \langle d_{BC}^2 \rangle - \langle d_{BC} \rangle^2 \\ &= x(1-x)(a_1^{**} - a^{**2}). \end{aligned}$$

The compact form above arises because one sublattice is always occupied by C-type atoms. The simple expressions (11) also reveal the connections between different experimentally measurable quantities. The topological rigidity constants in (7)–(11) can be taken as parameters characterizing the EXAFS results and *determined from experiment*. For example, in the case of $\text{Ga}_{1-x}\text{In}_x\text{As}$, from the nearest-neighbor distance EXAFS measurement, we can fit the value of a^{**} to be 0.8, which corresponds to $\beta/\alpha = 0.12$, which is smaller than the values for either GaAs or InAs as given in Table I. We then use $\beta/\alpha = 0.12$ to determine *all* the topological rigidity parameters. The Kirkwood model gives the corresponding a_1^{**} to be 0.57 and b^{**} to be 0.40.¹¹ In Fig. 1 we plot the analytic results from our theory and results from EXAFS experiments. The length distributions shown in the right panel are approximately Gaussian, whose centers and widths are given by Eqs. (11). The agreement shows that our model does grasp the main features of the problem, and produces the characteristic Z plot with two *parallel* lines for the mean AC and BC bond lengths. Such a straight line Z plot arises if and only if the variation in the force constants can be neglected. We will discuss how this applies to $\text{Ga}_{1-x}\text{In}_x\text{As}$ in the next section. In the perfectly floppy limit when the lattice has no effect, $a^{**} = 0$, and the two parallel lines in the Z plot become flat and independent of composition x . In the

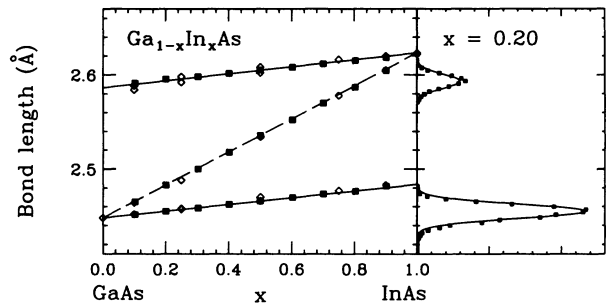


FIG. 1. The left panel compares the experimental results of Mikkelsen and Boyce (Ref. 2) (open symbols) for $\text{Ga}_{1-x}\text{In}_x\text{As}$ with simulation results using the Kirkwood potential with $a^{**} = 0.8$ corresponding to $\beta/\alpha = 0.12$ (solid symbols) and straight lines from the theory given by Eq. (7). The right panel shows our computer simulation results on a 8000-atom sample, with periodic boundary conditions, for the length probability distribution of nearest-neighbor Ga-As and In-As bonds for $x = 0.2$. The solid curves are Gaussians with centers, widths, and weights determined from Eqs. (7) and (8) in the text. Force constant disorder is ignored.

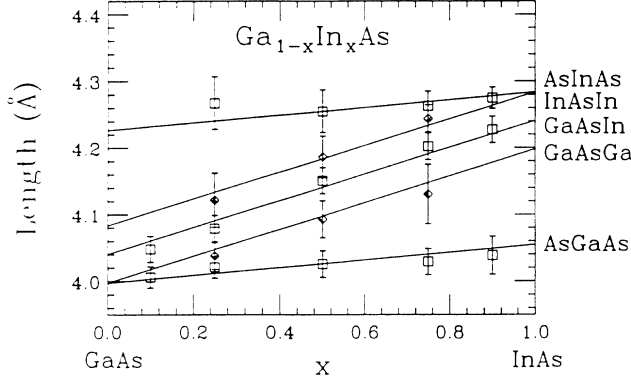


FIG. 2. The next-nearest-neighbor distance for $\text{Ga}_{1-x}\text{In}_x\text{As}$ with $a^{**} = 0.8$ and $b^{**} = 0.4$ using the Kirkwood potential with $\beta/\alpha = 0.12$ in Eq. (9). The experimental points are from Ref. 2. Force constant disorder is ignored.

perfectly rigid limit, which is unobtainable in practice, $a^{**} = 1$, and all three lines collapse onto the single line that characterizes Vegard's law. In these cases the mean length obeys Vegard's law, which arises because there is no variation in the force constants from site to site. Indeed even if clustering occurs, we still obtain Vegard's law if the force constants are the same.¹⁸ An extreme example of such clustering would be phase separation, where the law of mixtures obviously holds. Figure 2 shows the various mean next-nearest-neighbor distances calculated using Eq. (9) and compared to experiment. The new topological parameter needed, $b^{**} = 0.40$, is obtained from paper I, again using the ratio $\beta/\alpha = 0.12$ that is needed to give $a^{**} = 0.80$. Therefore there are no new parameters introduced to obtain the lines shown in Fig. 2. The results shown in Figs. 1 and 2 are obtained with the input of three quantities, the lattice parameters for GaAs and InAs and a single value of β/α or equivalently a^{**} . The three parallel lines in Fig. 2 for the mean *second*-neighbor distances Ga-As-Ga, Ga-As-In, and In-As-In are controlled by the single parameter b^{**} in Eq. (9). The two parallel lines for the mean As-Ga-As and As-In-As distances are controlled by the parameter a^{**} in Eq. (9). The ratio of the slopes of these two sequences of parallel straight lines is $(1 - a^{**})/(1 - \frac{3}{4}b^{**}) = 3.50$. These sets of parallel straight lines are a very striking feature of Fig. 2. Note that the ratio of the slopes of the two parallel lines in Fig. 2 for the next-nearest neighbors is $\sqrt{\frac{8}{3}}$, just the scale factor between the mean nearest- and next-nearest-neighbor distances. The ratio of the vertical spacing adjacent parallel lines in the set of three

to the vertical spacing between the two parallel lines is $8a^{**}/3b^{**} = 5.33$, which is a universal constant within the Kirkwood model. We clearly get good agreement between theory and experiment in Figs. 1 and 2, and the approach used here clearly identifies the general model-independent features in the mean nearest-neighbor and next-nearest-neighbor distances. An unsatisfactory feature of the approach used in this section is the necessity to obtain the single parameter a^{**} from EXAFS experiments.

B. Effective-medium approximation

When there is disorder not only in the atomic sizes, but also in the force constants, an analytic solution of the model is not possible. However, we will see that force constant disorder produces extremely small effects, like bowing, that are hard to observe experimentally. The effective-medium approximation (EMA) we use here has been applied by Thorpe and co-workers¹⁷⁻¹⁹ to other similar problems. The essential idea is to replace the particular environment around an atom with an average or effective environment that is obtained self-consistently. This kind of approximation becomes exact in the dilute limits, when either x or $(1 - x)$ is small. In this scheme, the rigidity and correlation information are contained in the topological rigidity constants which control the quantities of interest.

We give the main results and leave the derivation, which closely follows previous work on central force networks, to interested readers.¹⁷⁻¹⁹ For compactness the results are given in the reduced variables d defined in Eq. (10), and α denotes the force constant of the effective medium, with $\alpha_e = \alpha/a^{**}$ and $\alpha'_e = \alpha_e - \alpha$,

$$\begin{aligned} \langle d \rangle &= x + x(1-x)F_d, \\ \langle d_{AC} \rangle &= \frac{x\alpha_e\alpha'_e\alpha_{BC}}{\alpha(\alpha'_e + \alpha_{AC})(\alpha'_e + \alpha_{BC})}, \end{aligned} \quad (12)$$

$$\begin{aligned} \langle d_{BC} \rangle &= 1 - \frac{(1-x)\alpha_e\alpha'_e\alpha_{AC}}{\alpha(\alpha'_e + \alpha_{AC})(\alpha'_e + \alpha_{BC})}, \\ \varepsilon &= \frac{1}{2}\sqrt{\alpha_{AC}\alpha_{BC}}x(1-x)(L_{BC}^0 - L_{AC}^0)^2F_\varepsilon, \end{aligned}$$

where

$$F_d = \frac{\alpha_e\alpha'_e(\alpha_{BC} - \alpha_{AC})}{\alpha(\alpha'_e + \alpha_{AC})(\alpha'_e + \alpha_{BC})} \quad (13)$$

and

$$F_\varepsilon = \frac{F_d\sqrt{\alpha_{AC}\alpha_{BC}}}{\alpha_{BC} - \alpha_{AC}}. \quad (14)$$

The fluctuations are given by

$$\begin{aligned} \langle d_{AC}^2 \rangle - \langle d_{AC} \rangle^2 &= \langle d_{BC}^2 \rangle - \langle d_{BC} \rangle^2 \\ &= \frac{x(1-x)\{[\alpha_{AC}\alpha_{BC}\alpha_e^2]/[\alpha(\alpha'_e + \alpha_{AC})^2(\alpha'_e + \alpha_{BC})]\}^2}{a^{**2}/(a_1^{**} - a^{**2}) + [(\alpha - \alpha_{AC})(\alpha - \alpha_{BC})]/[(\alpha'_e + \alpha_{AC})(\alpha'_e + \alpha_{BC})]}, \\ \langle d^2 \rangle - \langle d \rangle^2 &= \frac{x(1-x)\{[\alpha_{AC}\alpha_{BC}\alpha_e]/[\alpha(\alpha'_e + \alpha_{AC})(\alpha'_e + \alpha_{BC})]\}^2 a_1^{**}/(a_1^{**} - a^{**2})}{a^{**2}/(a_1^{**} - a^{**2}) + [(\alpha - \alpha_{AC})(\alpha - \alpha_{BC})]/[(\alpha'_e + \alpha_{AC})(\alpha'_e + \alpha_{BC})]}. \end{aligned} \quad (15)$$

In the above equations, all the quantities have been previously defined except for the strain energy per site ε , which is the expectation value of the potential (1). In the limit of no force constant disorder Eq. (12) gives the exact result

$$\varepsilon = \frac{1}{2}\sqrt{\alpha_{AC}\alpha_{BC}} x(1-x)(L_{BC}^0 - L_{AC}^0)^2(1-a^{**}). \quad (16)$$

Indeed all the quantities in the EMA results (12)–(15) give back the previously found exact results in the limit of no force constant disorder. The force constants α and β are chosen from Table I, with β for the ACB angle taken to be the arithmetic mean of the values for the ACA and BCB bonds. The β force constants for the ACA and CAC bonds are set equal and also for the BCB and CBC angles, and obtained from Table I. As the EMA results are also exact in the dilute limits of small concentrations x or $(1-x)$, we have considerable confidence that the EMA provides a good overall description. Although the force constants β do not explicitly appear in the EMA, they are needed to evaluate the topological rigidity parameters, for which purpose we make a virtual crystal approximation for both α and β . The results are not sensitive to this as can be seen by the good agreement between the simulation results and the EMA in Figs. 3 and 4, where we have plotted the EMA against results obtained from computer simulations. The agreement with the simulations is seen to be excellent, and the variation in force constants produces a bowing of the curves, although this effect is quite small even for $\text{Zn}_{1-x}\text{Cd}_x\text{Te}$ which has a large difference in the angular force constants especially as can be seen from Table I. We compare the results for $\text{Ga}_{1-x}\text{In}_x\text{As}$ and $\text{Zn}_{1-x}\text{Cd}_x\text{Te}$ with experimental EXAFS and x-ray diffraction data in Figs. 3 and 4. The agreement is very good for $\text{Zn}_{1-x}\text{Cd}_x\text{Te}$ but less good for $\text{Ga}_{1-x}\text{In}_x\text{As}$, where a better agreement is obtained in Fig. 1 with the more empirical approach used in the previous section, with the variation in force constants ignored. Nevertheless, the overall agreement with experiment in Figs. 1–4 is rather satisfactory. Our

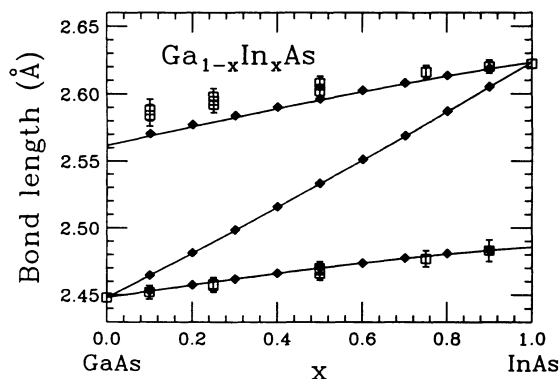


FIG. 3. The Z plot for $\text{Ga}_{1-x}\text{In}_x\text{As}$. Solid lines are from the effective-medium approximation. Solid symbols are from computer simulation using the Kirkwood potential with parameters taken from Table I. The open symbols with error bars are experimental EXAFS results (Ref. 2).

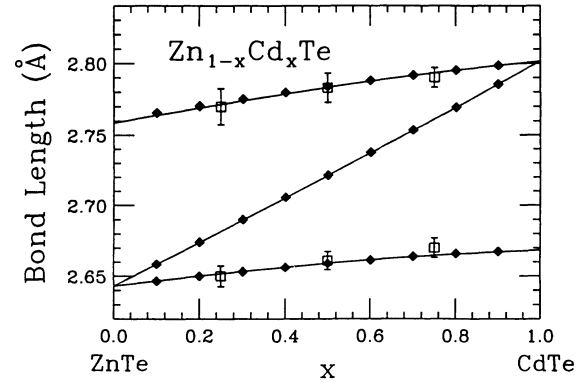


FIG. 4. The Z plot for $\text{Zn}_{1-x}\text{Cd}_x\text{Te}$. Solid lines are from the effective-medium approximation. Solid symbols are from computer simulation using the Kirkwood potential with parameters taken from Table I. Open symbols with error bars are experimental EXAFS results (Ref. 5).

main point is the insensitivity to the actual values of the various force constants, and the dominant role played by the topological rigidity parameters, whose value is largely determined by geometry. We note that Végard's law is *not* obeyed when the force constants α and β are different for AC and BC bonds in the pure binary systems, as seen by (12).

In most semiconductor alloys, the difference in the ratio of force constants, β/α , is modest as seen from Table I. This leads to very small deviations from Végard's law in the experimental data. But in general, Végard's law is not obeyed, and the question is always how large the deviations are.

IV. APPLICATIONS

Out of the 36 possible pseudobinary alloys that could be formed from Zn, Cd, Hg, P, As, Sb, and Al, Ga, In, Si, Ge, Sn, we study 29 of them (see Table II), for which force constants can be extracted from experimental data. We use the Kirkwood model in the effective-medium approximation described in the previous section.

It is easy to solve the effective-medium equations in the previous section using the interpolation formula for a^{**} given in paper I. As an example, we plot the Z curves for $\text{Ga}_x\text{In}_{1-x}\text{As}$ in Fig. 3 and $\text{Zn}_{1-x}\text{Cd}_x\text{Te}$ in Fig. 4. All the curves are straight lines plus a small bowing, as in the following description,

$$L = xp_1 + (1-x)p_2 + x(1-x)p_3, \quad (17)$$

where p_1 is the length at $x = 1$, and p_2 at $x = 0$, and p_3 denotes the bowing of the curve. Values of p_1 , p_2 , and p_3 are given in Table II, from the EMA.

We can also derive *analytic* values for these three parameters from the EMA equations, assuming the bowing to be small. Denote $\bar{\alpha} = (\alpha_{AC} + \alpha_{BC})/2$, and $\bar{\beta} = (\beta_{AC} + \beta_{BC})/2$. For an AC -type bond,

TABLE II. Length parameters (in Å) for $(A_{1-x}B_x)C$ or $C(A_{1-x}B_x)$ for use in expression (17) for the mean lengths.

	$\langle L_{AC} \rangle$			$\langle L_{BC} \rangle$			$\langle L \rangle$		
	p_1	p_2	p_3	p_1	p_2	p_3	p_1	p_2	p_3
AlP _{1-x} As _x	2.3846	2.3658	0.0051	2.4509	2.4171	0.0046	2.4509	2.3658	-0.0101
AlP _{1-x} Sb _x	2.4175	2.3658	0.0271	2.6559	2.5257	0.0225	2.6559	2.3658	-0.0537
AlAs _{1-x} Sb _x	2.5005	2.4509	0.0077	2.6559	2.5859	0.0074	2.6559	2.4509	-0.0127
GaP _{1-x} As _x	2.3851	2.3601	0.0019	2.4479	2.4189	0.0019	2.4479	2.3601	-0.0022
GaP _{1-x} Sb _x	2.4268	2.3601	0.0133	2.6396	2.5308	0.0120	2.6396	2.3601	-0.0294
GaAs _{1-x} Sb _x	2.4965	2.4479	0.0051	2.6396	2.5711	0.0048	2.6396	2.4479	-0.0150
InP _{1-x} As _x	2.5597	2.5412	0.0012	2.6233	2.5999	0.0013	2.6233	2.5412	-0.0036
InP _{1-x} Sb _x	2.5952	2.5412	0.0082	2.8056	2.7240	0.0084	2.8056	2.5412	-0.0193
InAs _{1-x} Sb _x	2.6660	2.6233	0.0030	2.8056	2.7546	0.0030	2.8056	2.6233	-0.0054
Ga _{1-x} Al _x P	2.3623	2.3601	-0.0002	2.3658	2.3643	-0.0002	2.3658	2.3601	0.0005
Ga _{1-x} Al _x As	2.4488	2.4479	0.0000	2.4509	2.4500	0.0000	2.4509	2.4479	0.0000
Ga _{1-x} Al _x Sb	2.6446	2.6396	0.0003	2.6567	2.6517	0.0003	2.6567	2.6396	0.0002
Al _{1-x} In _x P	2.3968	2.3658	0.0194	2.5412	2.4692	0.0171	2.5412	2.3658	-0.0228
Al _{1-x} In _x As	2.4881	2.4509	0.0115	2.6233	2.5638	0.0108	2.6233	2.4509	-0.0111
Al _{1-x} In _x Sb	2.6911	2.6567	0.0068	2.8056	2.7594	0.0065	2.8056	2.6567	-0.0053
Ga _{1-x} In _x P	2.4009	2.3601	0.0149	2.5412	2.4790	0.0133	2.5412	2.3601	-0.0073
Ga _{1-x} In _x As	2.4857	2.4479	0.0128	2.6233	2.5616	0.0119	2.6233	2.4479	-0.0116
Ga _{1-x} In _x Sb	2.6791	2.6396	0.0106	2.8056	2.7517	0.0097	2.8056	2.6396	-0.0043
ZnS _{1-x} Se _x	2.3645	2.3427	0.0002	2.4541	2.4279	0.0002	2.4541	2.3427	-0.0043
ZnS _{1-x} Te _x	2.4021	2.3427	-0.0014	2.6430	2.5678	-0.0018	2.6430	2.3427	-0.0174
ZnSe _{1-x} Te _x	2.4971	2.4541	-0.0013	2.6430	2.5977	-0.0014	2.6430	2.4541	-0.0036
CdS _{1-x} Se _x	2.5404	2.5193	0.0011	2.6206	2.5967	0.0011	2.6206	2.5193	-0.0016
CdS _{1-x} Te _x	2.5608	2.5193	0.0211	2.8085	2.7297	0.0216	2.8085	2.5193	-0.0159
CdSe _{1-x} Te _x	2.6493	2.6206	0.0120	2.8085	2.7604	0.0120	2.8085	2.6206	-0.0075
Zn _{1-x} Cd _x S	2.3784	2.3427	-0.0005	2.5193	2.4795	-0.0006	2.5193	2.3427	-0.0046
Zn _{1-x} Cd _x Se	2.4904	2.4541	0.0010	2.6206	2.5827	0.0010	2.6206	2.4541	-0.0006
Zn _{1-x} Cd _x Te	2.6697	2.6430	0.0133	2.8085	2.7644	0.0124	2.8085	2.6430	-0.0046
Zn _{1-x} Hg _x Te	2.6692	2.6430	0.0113	2.7955	2.7583	0.0101	2.7955	2.6430	-0.0004
Hg _{1-x} Cd _x Te	2.7976	2.7955	0.0001	2.8085	2.8060	0.0001	2.8085	2.7955	-0.0003

$$\begin{aligned}
p_1 &= L_{AC}^0 + \frac{(L_{BC}^0 - L_{AC}^0)}{1 + [(a^{**} - 1)\alpha_{AC}]/[a^{**}\alpha_{BC}]}, \\
p_2 &= L_{AC}^0, \\
p_3 &= \left[(1 - a^{**})^2 \left(\frac{\alpha_{BC} - \alpha_{AC}}{\bar{\alpha}} \right) \right. \\
&\quad \left. + \frac{\bar{\beta}}{\bar{\alpha}} (a^{**} - a_1^{**}) \left(\frac{\beta_{BC} - \beta_{AC}}{\bar{\beta}} \right) \right] (L_{BC}^0 - L_{AC}^0).
\end{aligned} \tag{18}$$

In the expression for p_1 , the topological rigidity parameter is evaluated at α_{BC} and β_{BC} , while in the expression for p_3 , the topological rigidity parameters are evaluated at $\bar{\alpha}$ and $\bar{\beta}$. For BC -type bonds, the parameter p_3 takes the same form, but x and $(1-x)$ are interchanged and AC and BC are switched in Eqs. (17) and (18). Similar results and parametrization has recently been used by Schabel and Martins,²⁰ who have produced extensive results for the pseudobinary alloys using the Keating potential. Their results and ours for both the nearest-neighbor and next-nearest-neighbor lengths are in general agreement. They also obtain sets of nearly parallel lines for the mean lengths from their computer simulation results. Our work explains the underlying origin of these sets of parallel lines. The deviations from

parallelism and the bowing are not identical as there are differences between the Kirkwood model and the Keating model at this level of sophistication, and we regard neither as being very reliable. Comparison between results for the Keating model²⁰ and the Kirkwood model in this paper, for any particular compound, gives a sense of how stable the results for the bowing of the Z curves are.

For the *overall* mean average length,

$$\begin{aligned}
p_1 &= L_{BC}^0, \\
p_2 &= L_{AC}^0, \\
p_3 &= (1 - a^{**}) \left(\frac{\alpha_{BC} - \alpha_{AC}}{\bar{\alpha}} \right) (L_{BC}^0 - L_{AC}^0),
\end{aligned} \tag{19}$$

where the argument of a^{**} involves $\bar{\alpha}$ and $\bar{\beta}$. It is interesting to analyze the approximate expressions above. We can see that the bowing of the curves for AC and BC are in the same sense and depend on *both* the differences of α and β for the two binary components in (18). However, the bowing of the overall average length only depends on the difference of central forces α in (19). For most semiconductor alloys, the bowing of the overall length average (lattice parameter) and the AC and BC length averages go in opposite directions, i.e., the angular force difference dominates the bowing in the mean AC and BC length

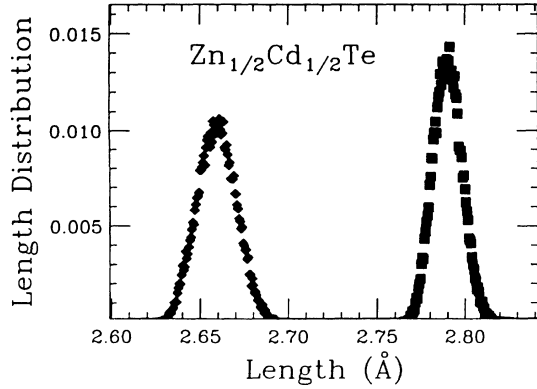


FIG. 5. The nearest-neighbor length distribution for Zn-Te and Cd-Te bonds in $\text{Zn}_{0.5}\text{Cd}_{0.5}\text{Te}$ from computer simulation using the Kirkwood potential with parameters taken from Table I.

averages, as in Fig. 4 for $\text{Zn}_{1-x}\text{Cd}_x\text{Te}$.

The nearest-neighbor length distribution is approximately Gaussian as can be seen in Fig. 1. Figure 5 shows the distribution of nearest-neighbor lengths in $\text{Zn}_{0.5}\text{Cd}_{0.5}\text{Te}$. There is barely any overlap between the two peaks, contrary to the situation in metal alloys.¹⁶ This is mainly due to the low nearest-neighbor coordination (4 compared to 12 in the fcc lattice), where the different distributions often overlap. The widths of AC and BC length distributions is not exactly the same because of the difference in force constants. We should point it out that our EMA does not give good results for the width of the distribution when there is clustering in the alloy.

V. CONCLUSIONS

We have studied the structure of the pseudobinary $(A_{1-x}B_x)C$ semiconducting alloys by applying the ex-

act solution for the quaternary system found in paper I, with no variation in the force constants. An effective-medium theory has been developed and applied to these pseudobinary compounds, when there is variation in the force constants. All our theoretical results have been checked against computer simulations. We find sets of straight lines, whose slopes are determined by the topological rigidity parameters, when there is no disorder in the force constants. These topological rigidity parameters are only weakly dependent on the atomic force constants. Force constant disorder produces only a slight bowing that is just discernable experimentally in a few pseudobinaries like $\text{Zn}_{1-x}\text{Cd}_x\text{Te}$. Our results show that detailed model calculations are not required (if the small bowing is neglected) and the single topological rigidity parameter ($a^{**} = 2b^{**}$ in the region of physical interest) can be obtained from experiment.

ACKNOWLEDGMENTS

We should like to thank B. Bunker, S. D. Mahanti, and N. Mousseau for interesting discussions. This work was supported in part by the NSF under Grant No. DMR 9024955.

APPENDIX

In this appendix we examine the Kirkwood model¹³ and the Keating model¹⁴ together in a unified notation. Recall the form of the elastic energy for the Kirkwood model (3)

$$V_{\text{Kirkwood}} = \frac{\alpha}{2} \sum_{\langle ij \rangle} (\hat{\mathbf{r}}_{ij} \cdot \mathbf{u}_{ij})^2 + \frac{\beta}{8} \sum_{\langle ijkl \rangle} [\hat{\mathbf{r}}_{ij} \cdot \mathbf{u}_{il} + \hat{\mathbf{r}}_{il} \cdot \mathbf{u}_{ij} + \frac{1}{3} (\hat{\mathbf{r}}_{ij} \cdot \mathbf{u}_{ij} + \hat{\mathbf{r}}_{il} \cdot \mathbf{u}_{il})]^2, \quad (\text{A1})$$

where the notation is explained in the main text. The Keating model is written

$$V_{\text{Keating}} = \frac{\alpha}{2} \sum_{\langle ij \rangle} (\hat{\mathbf{r}}_{ij} \cdot \mathbf{u}_{ij})^2 + \frac{\beta}{8} \sum_{\langle ijkl \rangle} (\hat{\mathbf{r}}_{ij} \cdot \mathbf{u}_{il} + \hat{\mathbf{r}}_{il} \cdot \mathbf{u}_{ij})^2. \quad (\text{A2})$$

It can be seen that these two models are very similar except there are extra terms in the Kirkwood model. We can combine them in a single potential

$$V_{\lambda} = \frac{\alpha}{2} \sum_{\langle ij \rangle} (\hat{\mathbf{r}}_{ij} \cdot \mathbf{u}_{ij})^2 + \frac{\beta}{8} \sum_{\langle ijkl \rangle} \left[\hat{\mathbf{r}}_{ij} \cdot \mathbf{u}_{il} + \hat{\mathbf{r}}_{il} \cdot \mathbf{u}_{ij} + \frac{\lambda}{3} (\hat{\mathbf{r}}_{ij} \cdot \mathbf{u}_{ij} + \hat{\mathbf{r}}_{il} \cdot \mathbf{u}_{il}) \right]^2, \quad (\text{A3})$$

where $\lambda = 0$ gives the Keating model and $\lambda = 1$ gives the Kirkwood model.

The elastic modulus of the combined λ model can be found in the similar way to that used in Keating's original paper.¹⁴ The results are

$$\begin{aligned} C_{11} &= \frac{1}{4a} \left[\alpha + 3\beta - \frac{2\lambda\beta}{3} + \frac{\beta\lambda^2}{3} \right], \\ C_{12} &= \frac{1}{4a} \left[\alpha - \beta - \frac{2\lambda\beta}{3} + \frac{\beta\lambda^2}{3} \right], \\ C_{44} &= \frac{1}{4a} \left[\alpha + \beta - \frac{2\lambda\beta}{3} + \frac{\beta\lambda^2}{9} \right. \\ &\quad \left. - \frac{\{\alpha - \beta[1 - (\lambda/3)^2]\}^2}{\alpha + \beta(1 + \lambda/3)^2} \right], \end{aligned} \quad (\text{A4})$$

where $a = L_e/\sqrt{3}$. The frequency of the optical phonon at $\mathbf{k} = 0$ is

$$\omega_0 = \sqrt{\frac{4}{\mu} \left[\alpha + \beta \left(1 + \frac{\lambda}{3} \right)^2 \right]}. \quad (\text{A5})$$

The force constants in the models are chosen to fit the elastic modulus C_{11} and the bulk modulus $B = \frac{1}{3}(C_{11} + 2C_{12})$.¹⁵ We list in Table I the force constants for different semiconductor compounds which have the zincblende structure. We have also computed the topological rigidity parameters a^{**} , b^{**} and their derivatives for the

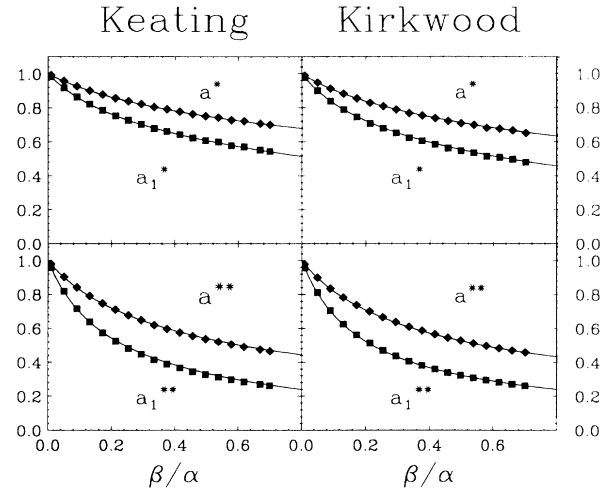


FIG. 6. A comparison of the topological rigidity constants a^* , a_1^* and a^{**} , a_1^{**} computed as lattice integrals for the Kirkwood and Keating models. The topological rigidity parameters a^* and a_1^* are used in paper III.

Keating model, using the lattice integrals given in Eq. (33) of paper I. The results are shown in Fig. 6. It can be seen that the topological rigidity parameters are very similar for these two models. We have also computed b^{**} and it is clear that $a^{**} \neq b^{**}/2$ for the Keating model, although it is still approximately true.

¹L. Végard, Z. Phys. **5**, 17 (1921).

²J. C. Mikkelsen, Jr. and J. B. Boyce, Phys. Rev. B **28**, 7130 (1983).

³J. C. Mikkelsen, Jr. and J. B. Boyce, Phys. Rev. Lett. **49**, 1412 (1982).

⁴J. B. Boyce and J. C. Mikkelsen, Jr., Phys. Rev. B **31**, 6903 (1985).

⁵A. Balzarotti, in *Ternary and Multinary Compounds*, edited by S. K. Deb and A. Zunger (Materials Research Society, Pittsburgh, 1987), p. 333.

⁶T. Sasaki, T. Onda, R. Ita, and N. Ogasawara, Jpn. J. Appl. Phys. **25**, 231 (1986).

⁷J. L. Martins and A. Zunger, Phys. Rev. B **30**, 6217 (1984).

⁸A. B. Chen and A. Sher, Phys. Rev. B **32**, 3695 (1985).

⁹C. K. Shih, W. E. Spicer, W. A. Harrison, and A. Sher, Phys. Rev. B **31**, 1139 (1985).

¹⁰M. Podgorny, M. T. Czyzyk, A. Balzarotti, P. Letardi, N. Motta, A. Kisiel, and M. Zimnal-Starnawska, Solid State Commun. **55**, 413 (1985).

¹¹Y. Cai and M. F. Thorpe, preceding paper, Phys. Rev. B **46**, 15 872 (1992).

¹²N. Mousseau and M. F. Thorpe, following paper, Phys. Rev. B **46**, 15 887 (1992).

¹³J. G. Kirkwood, J. Chem. Phys. **7**, 506 (1939).

¹⁴P. N. Keating, Phys. Rev. **145**, 637 (1966).

¹⁵*Semiconductors, Group III: Crystal and Solid State Physics*, Landolt-Bornstein, New Series, Vol. 22 (Springer-Verlag, Berlin, 1987).

¹⁶N. Mousseau and M. F. Thorpe, Phys. Rev. B **45**, 2015 (1992).

¹⁷Y. Cai, J. S. Chung, M. F. Thorpe, and S. D. Mahanti, Phys. Rev. B **42**, 8827 (1990).

¹⁸M. F. Thorpe and E. J. Garboczi, Phys. Rev. B **42**, 8405 (1990).

¹⁹M. F. Thorpe and W. Jin, S. D. Mahanti, Phys. Rev. B **40**, 10 294 (1989).

²⁰M. C. Schabel and J. L. Martins, Phys. Rev. B **43**, 11 873 (1992).